Supplemental Material
Electronic, vibrational, and electron-phonon coupling properties in $SnSe_2$ and SnS_2 under pressure

Gyanu Prasad Kafle,[1] Christoph Heil,[2] Hari Paudyal,[1] and Elena R. Margine[1,*]

[1] *Department of Physics, Applied Physics, and Astronomy, Binghamton University-SUNY, Binghamton, New York 13902, USA*
[2] *Institute of Theoretical and Computational Physics, Graz University of Technology, NAWI Graz, 8010 Graz, Austria*

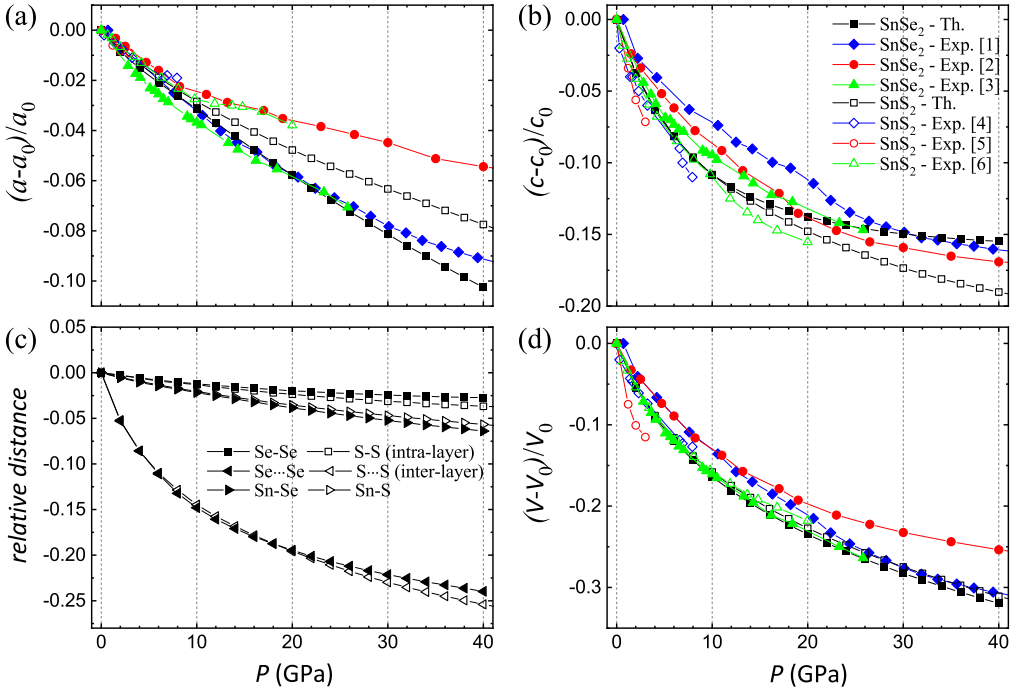

FIG. S1. Pressure dependence of the relative change of (a)-(b) lattice parameters a and c, (c) average bond lengths, and (d) volume per formula unit for $SnSe_2$ and SnS_2. Theoretical results are shown as black symbols and are compared with available experimental data [1–6].

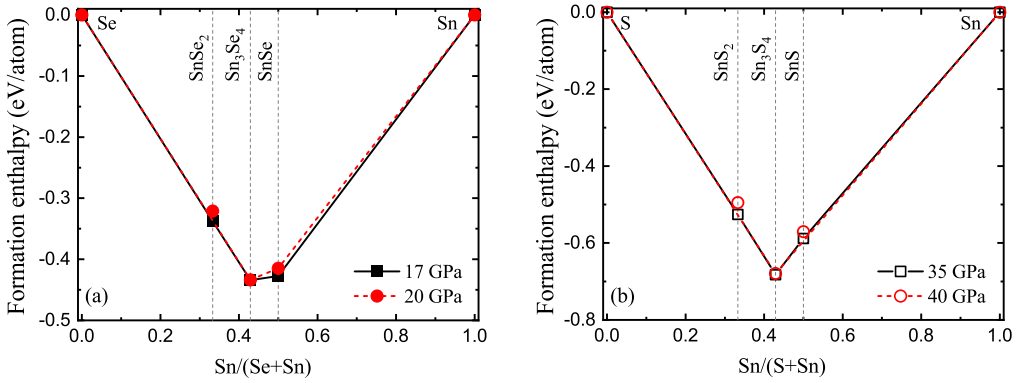

FIG. S2. Convex hulls of (a) Sn_xSe_y and (b) Sn_xS_y systems at various pressures.

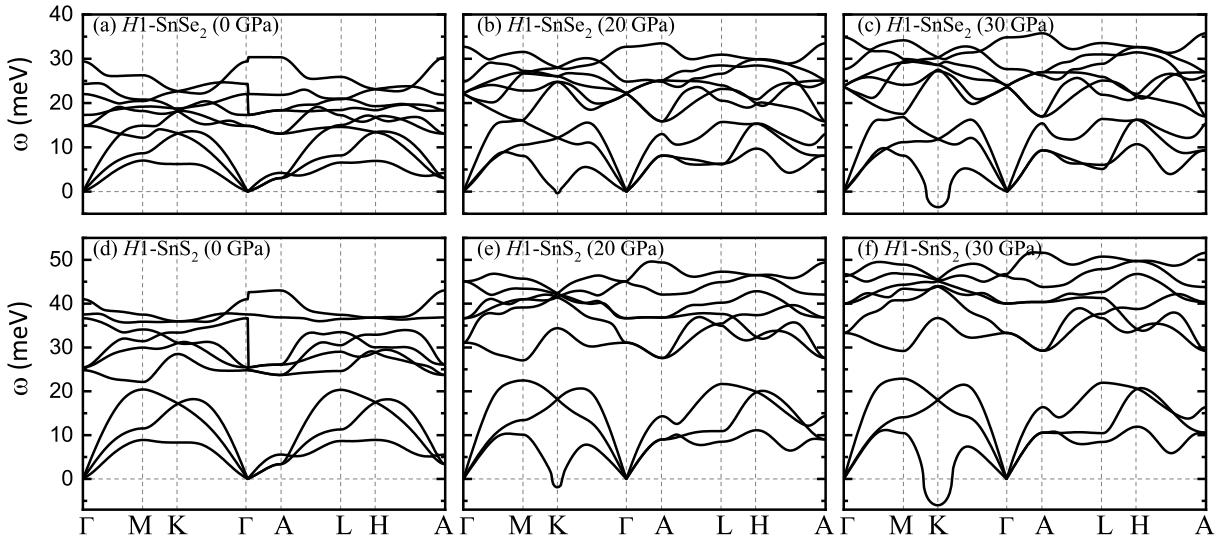

FIG. S3. Calculated phonon dispersion for the $H1$ structure in the $1 \times 1 \times 1$ unit cell of (a)-(c) $SnSe_2$ and (d)-(f) SnS_2 at 0, 20, and 30 GPa.

System	Phase	Space group	Eigenvector combination	ΔH (meV/atom)	Similarity factor	a (Å)	c (Å)	Wyckoff positions Sn	Wyckoff positions Se/S
$SnSe_2$	$H1$ (0 GPa)	164 P$\bar{3}$m1				3.86169	6.10587	1a (0.00000, 0.00000, 0.00000)	2d (0.33333, 0.66667, 0.23363)
	$H1$ (30 GPa)	164 P$\bar{3}$m1				3.54726	5.19218	1a (0.00000, 0.00000, 0.00000)	2d (0.33333, 0.66667, 0.30816)
	$H2$-1 (30 GPa)	147 P$\bar{3}$	e_1	-1.86477	0.4983	6.14654	5.17350	2d (0.33333, 0.66667, 0.95799)	6g (0.02978, 0.34880, 0.30584)
								1a (0.00000, 0.00000, 0.00000)	
	$H2$-2 (30 GPa)	157 P31m	e_2	-1.83621	0.2058	6.14662	5.17334	2b (0.33333, 0.66667, 0.97571)	3c (0.00000, 0.35864, 0.30583)
								1a (0.00000, 0.00000, 0.04855)	3c (0.00000, 0.69306, 0.69416)
SnS_2	$H1$ (0 GPa)	164 P$\bar{3}$m1				3.68056	5.88359	1a (0.00000, 0.00000, 0.00000)	2d (0.33333, 0.66667, 0.25197)
	$H1$ (30 GPa)	164 P$\bar{3}$m1				3.45051	4.84234	1a (0.00000, 0.00000, 0.00000)	2d (0.33333, 0.66667, 0.30146)
	$H2$-1 (30 GPa)	147 P$\bar{3}$	e_1	-1.30561	0.6158	5.96638	4.84894	2d (0.33333, 0.66667, 0.03189)	6g (0.97915, 0.32334, 0.30017)
								1a (0.00000, 0.00000, 0.00000)	
	$H2$-2 (30 GPa)	157 P31m	e_2	-1.31027	0.4223	5.96619	4.84884	2b (0.33333, 0.66667, 0.01870)	3c (0.00000, 0.31459, 0.30014)
								1a (0.00000, 0.00000, 0.96262)	3c (0.00000, 0.64879, 0.69986)
	$H2$-3 (30 GPa)	143 P3	$e_1 + e_2$	-1.32715	0.5887	5.97630	4.84268	1a (0.00000, 0.00000, 0.97419)	3d (0.99372, 0.31659, 0.30144)
								1b (0.33333, 0.66667, 0.02175)	3d (0.00628, 0.65620, 0.69856)
								1c (0.66667, 0.33333, 0.00407)	

TABLE S1. Space groups, lattice parameters, and Wyckoff positions of $SnSe_2$ and SnS_2 structures fully relaxed at the DFT level. The space groups were found with the SPGLIB tool [7] interfaced with the MAISE package [8] using a tolerance of 0.01. The lattice parameters are given for $H1$ at 0 GPa and 30 GPa, and for the $H2$ derivatives at 30 GPa. The $H2$ derivatives were constructed from the $\sqrt{3} \times \sqrt{3} \times 1$ $H1$ supercell by considering nonequivalent combinations of the e_1 and e_2 eigenvectors corresponding to the two nearly degenerate lowest-energy phonon modes A_{2g} and A_{2u}. Configuration $H2$-1 corresponds to atomic displacements along e_1, configuration $H2$-2 corresponds to atomic displacements along e_2, and configuration $H2$-3 corresponds to atomic displacements along a linear combination of the two eigenvectors. The similarity factor was calculated for each $H2$ derivative with respect to the undistorted $\sqrt{3} \times \sqrt{3} \times 1$ $H1$ supercell.

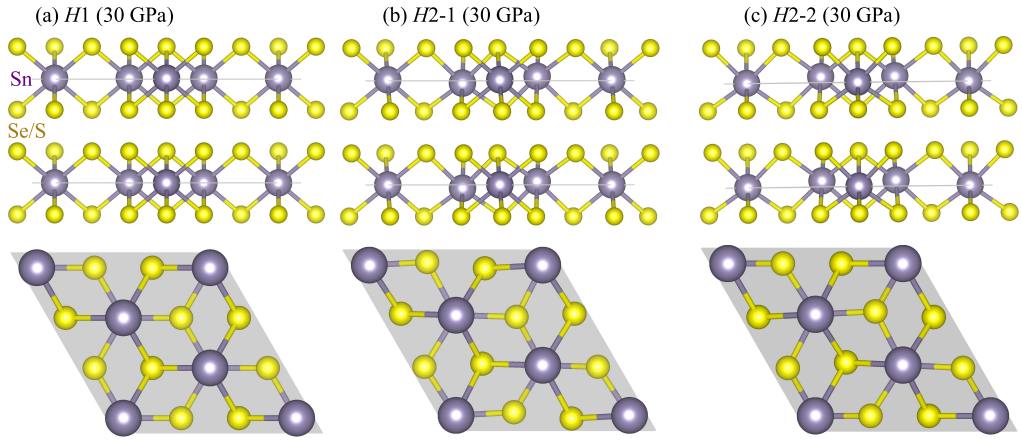

FIG. S4. Crystal structures (side and top view) for the (a) $H1$, (b) $H2$-1, and (c) $H2$-2 structures in the $\sqrt{3}\times\sqrt{3}\times1$ supercell of $SnSe_2$ and SnS_2, fully relaxed with the DFT at 30 GPa.

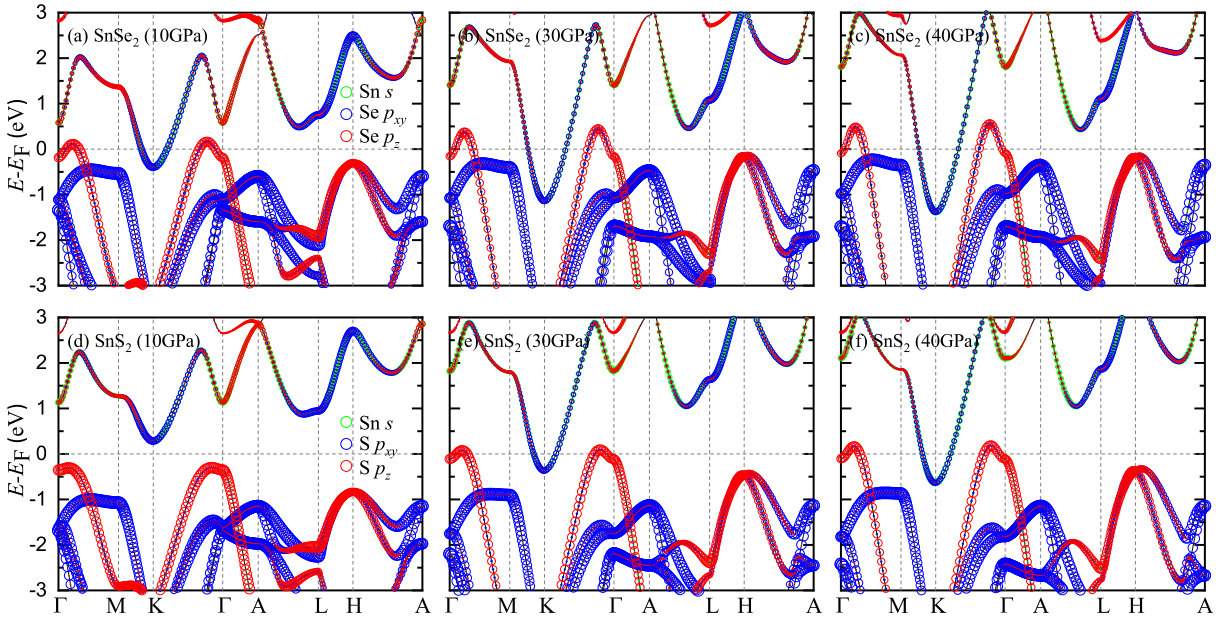

FIG. S5. Calculated band structure for the $H1$ structure in the $1\times1\times1$ unit cell of (a)-(c) $SnSe_2$ and (d)-(f) SnS_2 at 10, 30, and 40 GPa. The size of the symbols is proportional to the contribution of each orbital character.

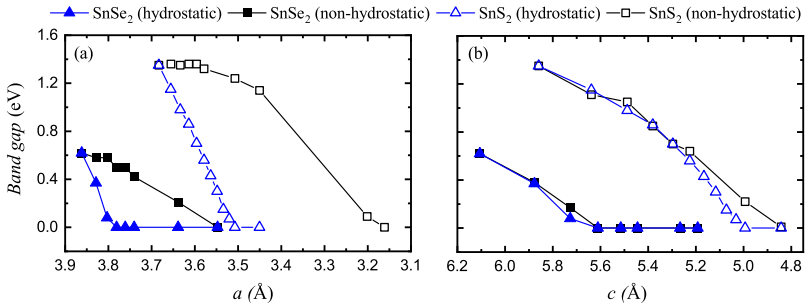

FIG. S6. Calculated band gap for the $H1$ structure in the $1\times1\times1$ unit cell of $SnSe_2$ and SnS_2 under hydrostatic and non-hydrostatic pressure as a function of lattice parameters (a) a and (b) c. In (a), c is kept fixed at $c = 6.10$ Å for $SnSe_2$ and $c = 5.86$ Å for SnS_2. In (b), a is kept fixed at $a = 3.86$ Å for $SnSe_2$ and $a = 3.68$ Å for SnS_2.

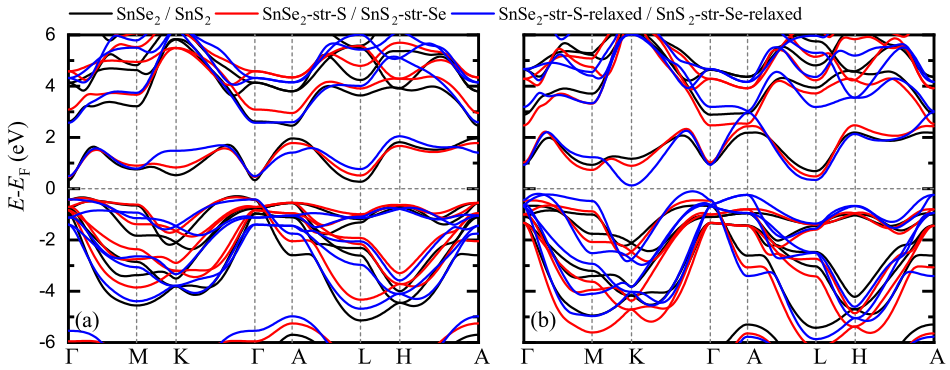

FIG. S7. Calculated band structure for the $H1$ structure in the $1 \times 1 \times 1$ unit cell of (a) $SnSe_2$, $SnSe_2$-str-S, and $SnSe_2$-str-S-relaxed and (b) SnS_2, SnS_2-str-Se, and SnS_2-str-Se-relaxed at 0 GPa.

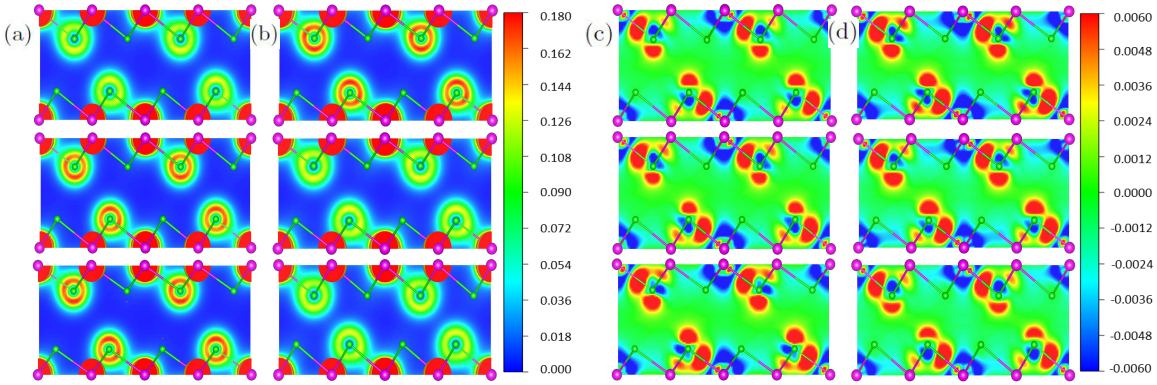

FIG. S8. Calculated (a) charge density and (c) charge density difference along the (110) plane for the $H1$ structure in the $1 \times 1 \times 1$ unit cell of $SnSe_2$, $SnSe_2$-str-S, and $SnSe_2$-str-S-relaxed (from top to bottom) at 0 GPa. Same for SnS_2, SnS_2-str-Se, and SnS_2-str-Se-relaxed in (b) and (d).

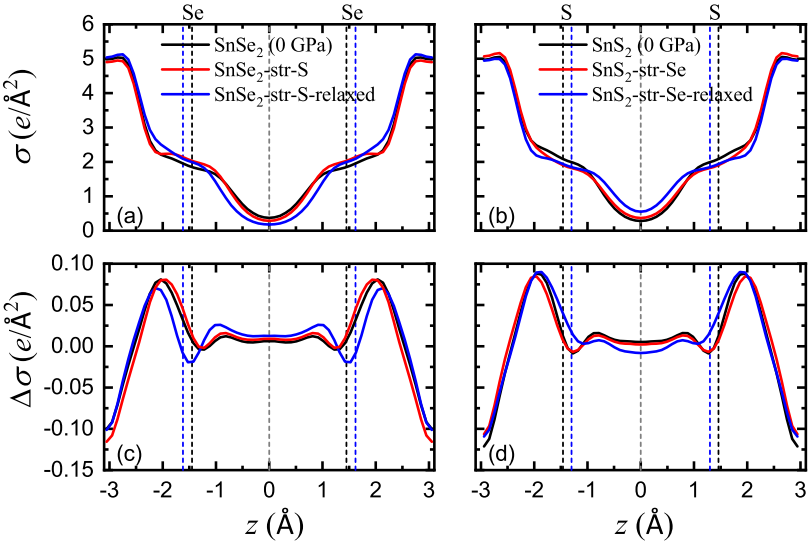

FIG. S9. Calculated (a) charge density and (c) charge density difference (in the x-y plane) as a function of the perpendicular direction z for the $H1$ structure in the $1 \times 1 \times 1$ unit cell of $SnSe_2$, $SnSe_2$-str-S, and $SnSe_2$-str-S-relaxed at 0 GPa. Same for SnS_2, SnS_2-str-Se, and SnS_2-str-Se-relaxed in (b) and (d). The vertical black and blue dashed lines represent the position of the Se/S atoms for $SnSe_2/SnS_2$ and $SnSe_2$-str-S-relaxed/SnS_2-str-Se-relaxed structures along c-axis, and the vertical gray dashed line represents the middle of van der Waals gap.

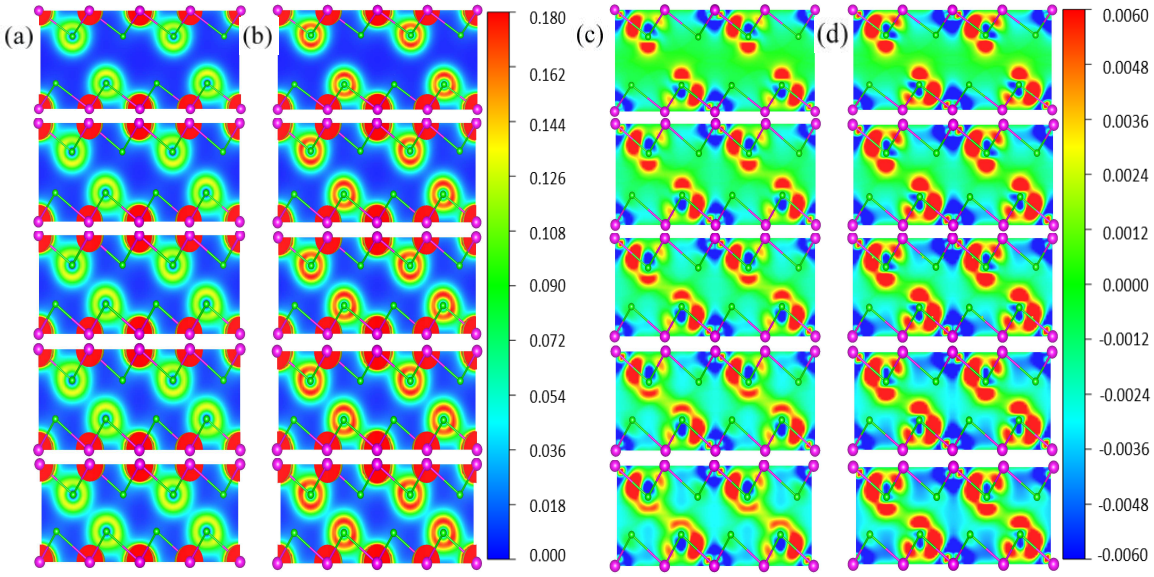

FIG. S10. Calculated (a) charge density and (c) charge density difference along the (110) plane for the $H1$ structure in the $1 \times 1 \times 1$ unit cell of $SnSe_2$ at various pressures. Same for SnS_2 in (b) and (d). The pressure order is 0, 10, 20, 30, and 40 GPa from top to bottom.

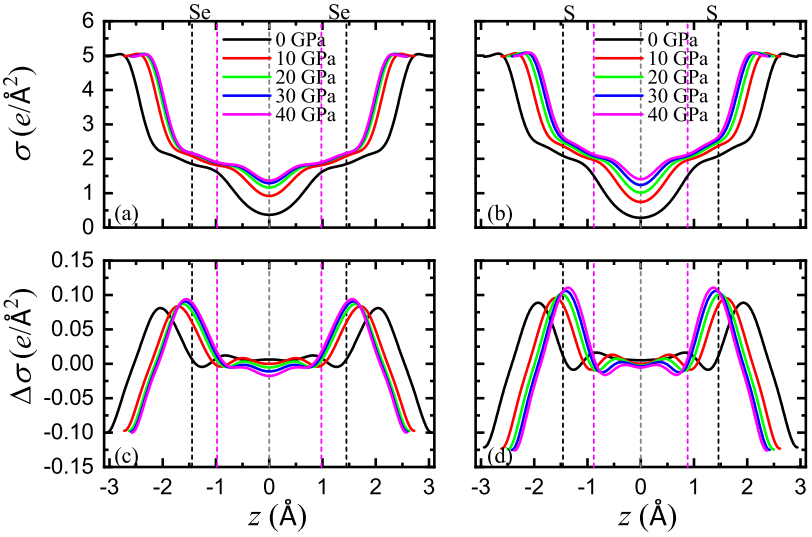

FIG. S11. Calculated (a) charge density and (c) charge density difference (in the x-y plane) as a function of the perpendicular direction z for the $H1$ structure in the $1 \times 1 \times 1$ unit cell of $SnSe_2$ at various pressures. Same for SnS_2 in (b) and (d). The vertical black and magenta dashed lines represent the position of the Se/S atoms for $SnSe_2/SnS_2$ structures along c-axis at 0 and 40 GPa, respectively, and the vertical gray dashed line represents the middle of van der Waals gap.

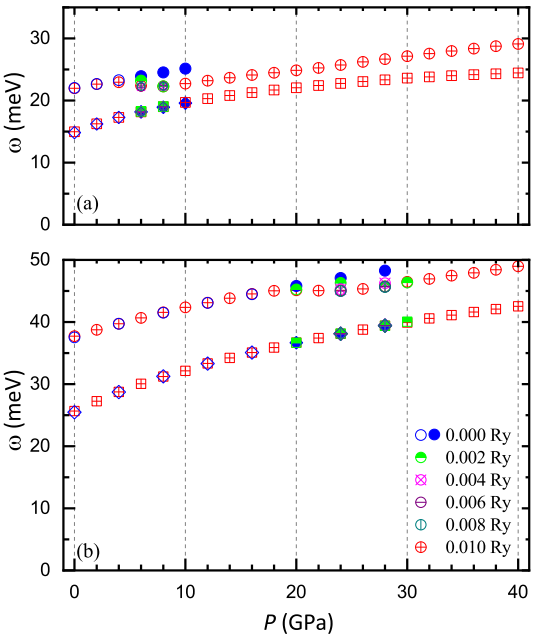

FIG. S12. Calculated frequency dependence of the Raman-active modes, A_{1g} and E_g, for the $H1$ structure in the $1 \times 1 \times 1$ unit cell of (a) $SnSe_2$ and (b) SnS_2 as a function of pressure using various smearing values. The data before and after the metalization (6 GPa in $SnSe_2$ and 20 GPa in SnS_2) using no smearing are shown as open and filled blue circles, respectively.

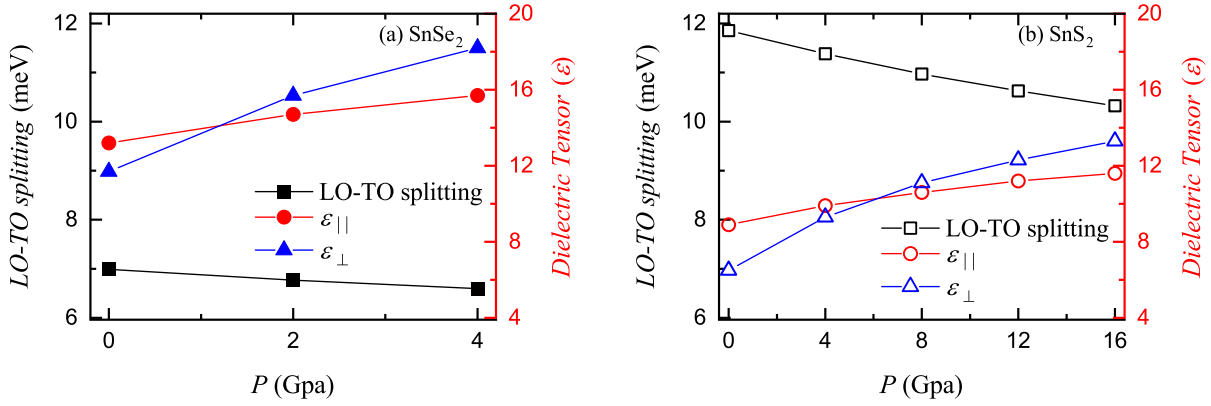

FIG. S13. Calculated LO-TO splitting, and in-plane ($\varepsilon_{\parallel}$) and out-of-plane ($\varepsilon_{\perp}$) dielectric tensors for the $H1$ structure in the $1 \times 1 \times 1$ unit cell of (a) $SnSe_2$ and (b) SnS_2 as a function of pressure.

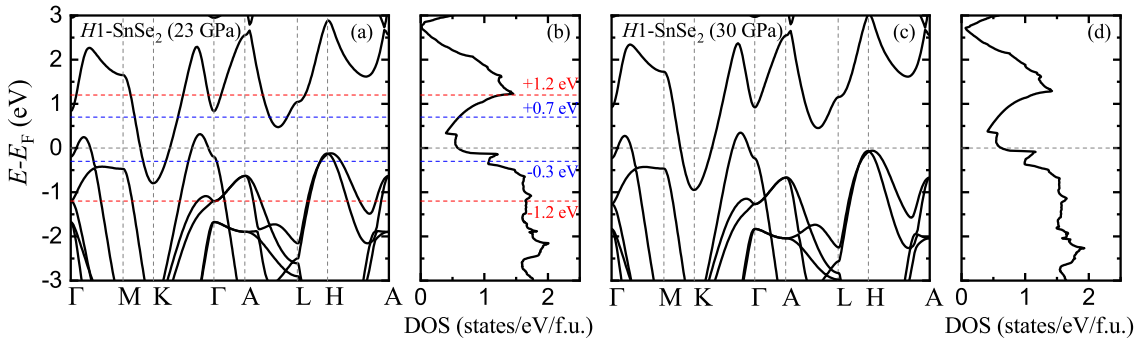

FIG. S14. Calculated band structure and DOS for the $H1$ structure in the $1 \times 1 \times 1$ unit cell of $SnSe_2$ at the experimental unit cell parameters at (a)-(b) 23 and (c)-(d) 30 GPa. The red and blue dashed lines represent rigid shifts of the Fermi level with respect to the original data.

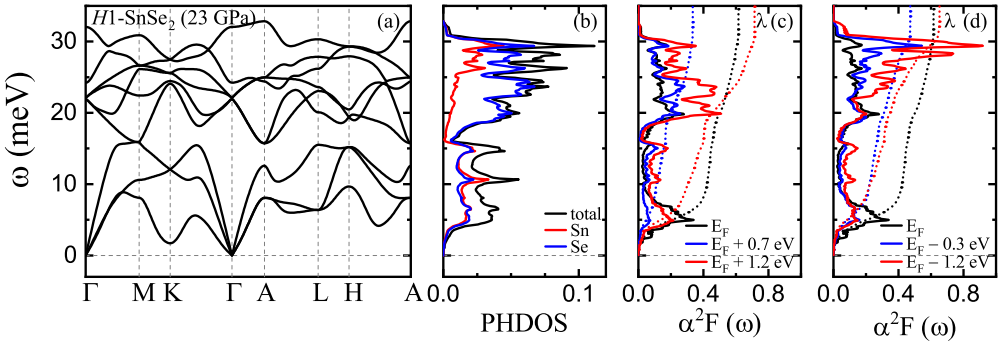

FIG. S15. Calculated (a) phonon dispersion, (b) PHDOS, and (c)-(d) Eliashberg spectral function $\alpha^2F(\omega)$ and e-ph coupling strength $\lambda(\omega)$ for the $H1$ structure in the $1 \times 1 \times 1$ unit cell of $SnSe_2$ at the experimental lattice parameters at 23 GPa. In (c) and (d), black lines show $\alpha^2F(\omega)$ and $\lambda(\omega)$ at the Fermi level, while red and blue lines show the same quantities for the rigid shifts in the Fermi level indicated in Fig. S14(a)-(b).

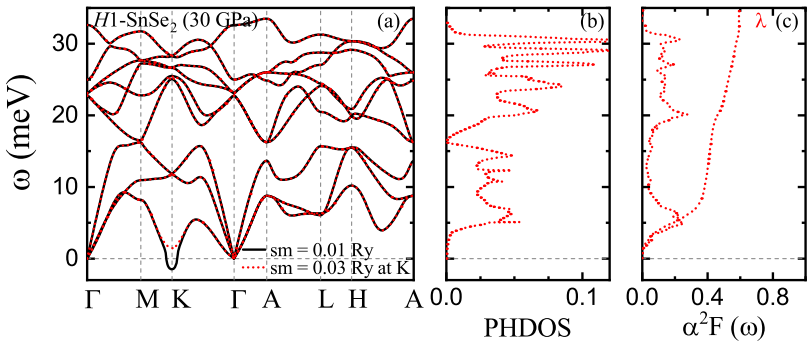

FIG. S16. Calculated (a) phonon dispersion, (b) PHDOS, and (c) Eliashberg spectral function $\alpha^2F(\omega)$, and e-ph coupling strength $\lambda(\omega)$ for the $H1$ structure in the $1 \times 1 \times 1$ unit cell of $SnSe_2$ at the experimental lattice parameters at 30 GPa. The black lines represent the phonon calculated with a smearing value of 0.01 Ry, while red lines with a smearing value of 0.03 Ry at the K-point in the BZ.

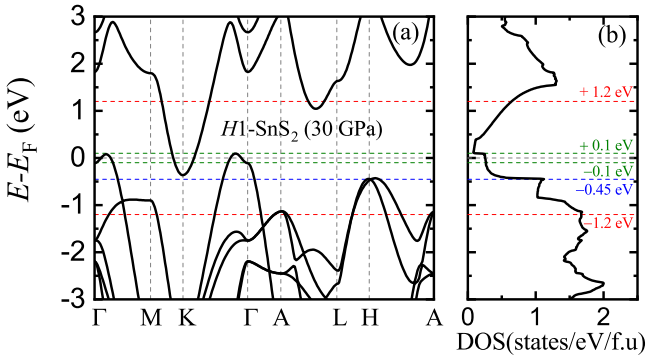

FIG. S17. Calculated (a) band structure and (b) DOS for the $H1$ structure in the $1 \times 1 \times 1$ unit cell of SnS_2 at 30 GPa. The red and blue dashed lines represent rigid shifts of the Fermi level with respect to the original data.

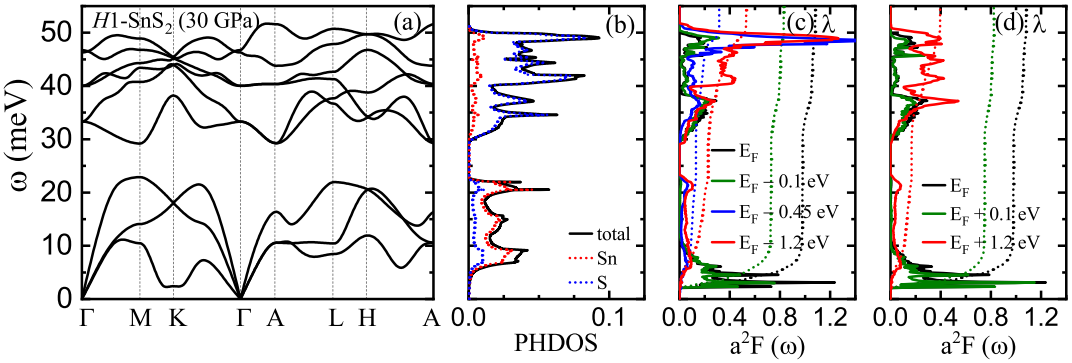

FIG. S18. Calculated (a) phonon dispersion, (b) PHDOS, and (c)-(d) Eliashberg spectral function $\alpha^2F(\omega)$, and e-ph coupling strength $\lambda(\omega)$ for the $H1$ structure in the $1 \times 1 \times 1$ unit cell of SnS_2 at 30 GPa. In (c) and (d), black lines show $\alpha^2F(\omega)$ and $\lambda(\omega)$ at the Fermi level, while red, blue and green lines show the same quantities for the rigid shifts in the Fermi level indicated in Fig. S17. The phonon is calculated with a smearing value of 0.04 Ry at the K-point in the BZ.

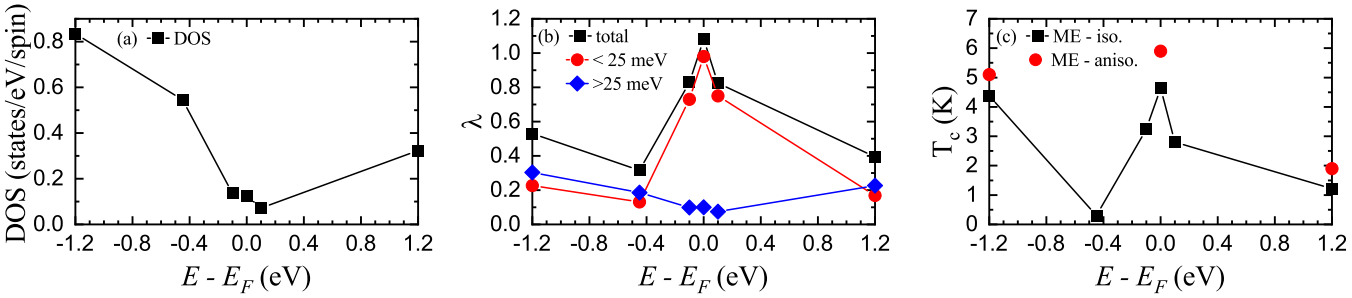

FIG. S19. Variations in (a) DOS at E_F, (b) λ, and (c) T_c as a function of a rigid shift of the Fermi level for the $H1$ structure in the $1 \times 1 \times 1$ unit cell of SnS_2 at 30 GPa. In (b), squares represent the total λ, while circles and rhombuses represent the contribution of the low- and high-energy modes. In (c), circles and squares represent the T_c obtained from the numerical solutions of the anisotropic and isotropic ME equations.

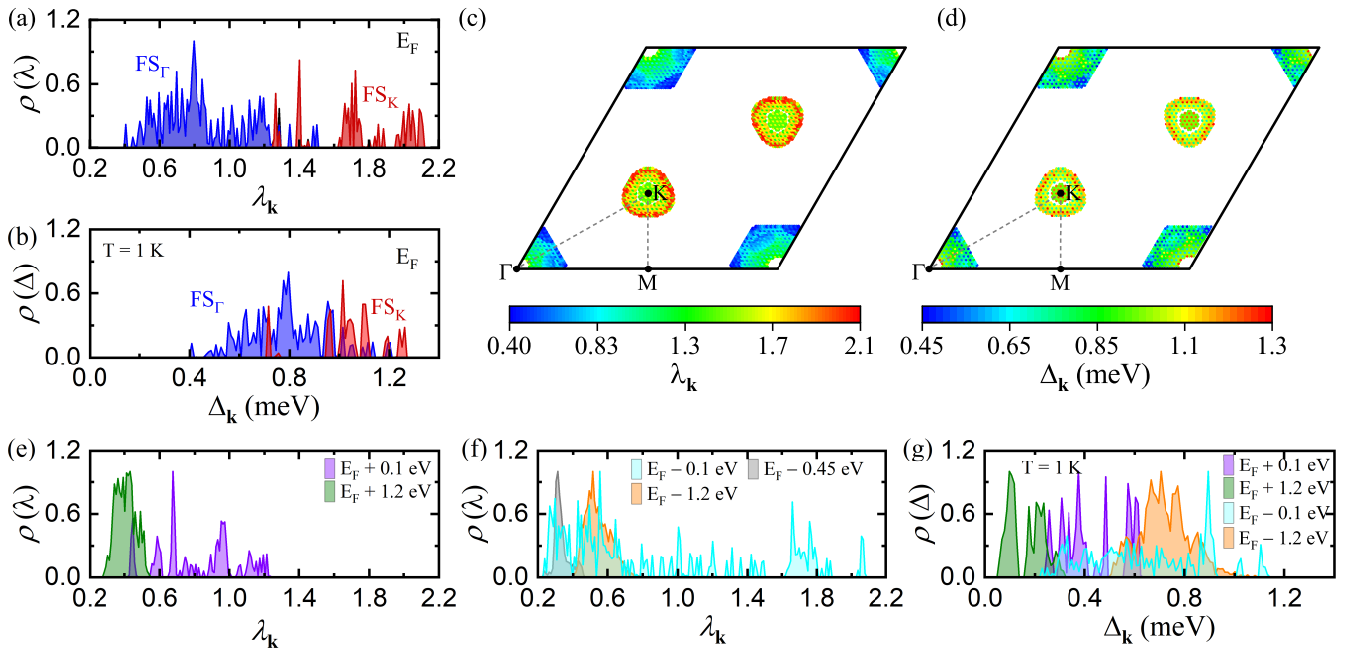

FIG. S20. Calculated superconducting properties for the $H1$ structure in the $1 \times 1 \times 1$ unit cell of SnS_2 at 30 GPa. Energy distribution of the (a) e-ph coupling strength $\lambda_{\mathbf{k}}$ and (b) superconducting gap $\Delta_{\mathbf{k}}$; color coded by FS sheets: Γ-centered holelike pocket FS_Γ (blue), and K-centered electronlike pocket FS_K (red). Momentum-resolved (c) e-ph coupling strength $\lambda_{\mathbf{k}}$ and (d) superconducting gap $\Delta_{\mathbf{k}}$ on the FS (top-view). Energy distribution of the (e) e-ph coupling strength $\lambda_{\mathbf{k}}$, and (f)-(g) superconducting gap $\Delta_{\mathbf{k}}$ at $T = 1$ K at various rigid shifts of the Fermi level with respect to the original data as shown in Fig. S17(a)-(b).

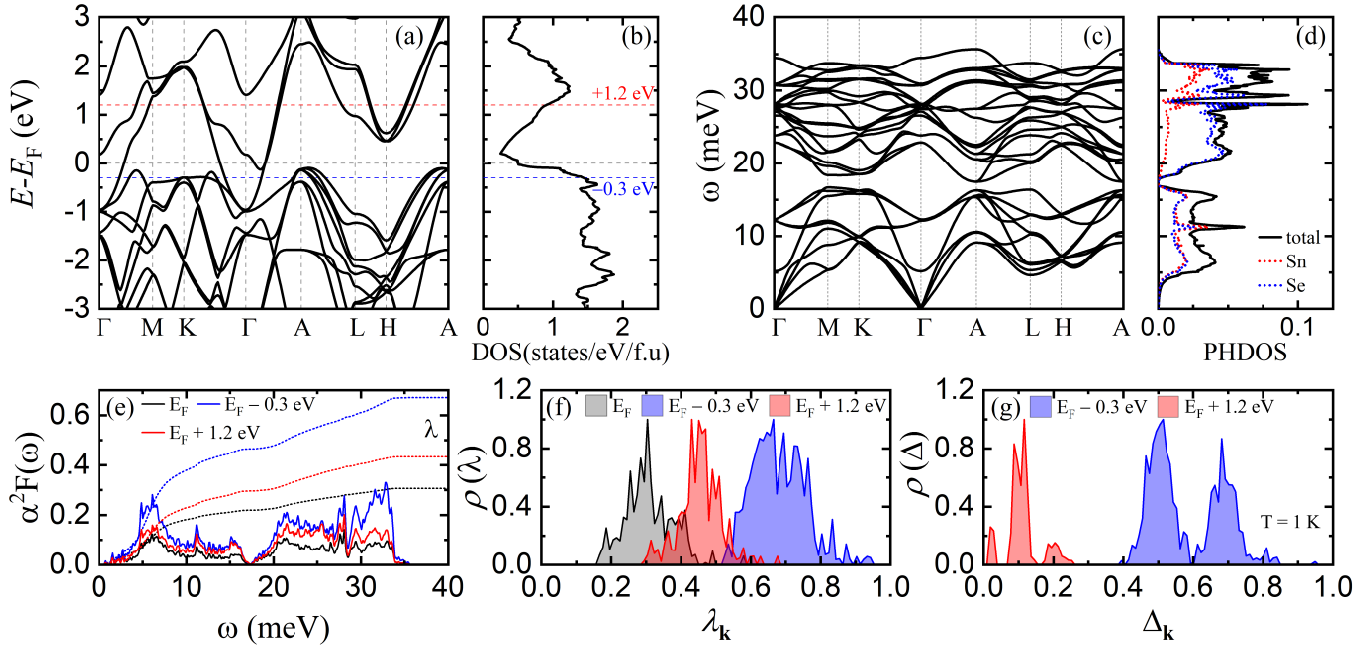

FIG. S21. Calculated (a) band structure, (b) DOS, (c) phonon dispersion, (d) PHDOS, (e) Eliashberg spectral function $\alpha^2F(\omega)$ and e-ph coupling strength $\lambda(\omega)$, (f) energy distribution of the e-ph coupling strength $\lambda_{\mathbf{k}}$, and (g) energy distribution of the superconducting gap $\Delta_{\mathbf{k}}$ at $T = 1$ K for the $H2$-1 structure in the $\sqrt{3} \times \sqrt{3} \times 1$ supercell of $SnSe_2$ at 30 GPa. In (e)-(g), black lines show the quantities at the Fermi level, while red and blue lines correspond to the rigid shifts in the Fermi level indicated in (a) and (b). Note that the DOS and PHDOS are plotted per formula unit.

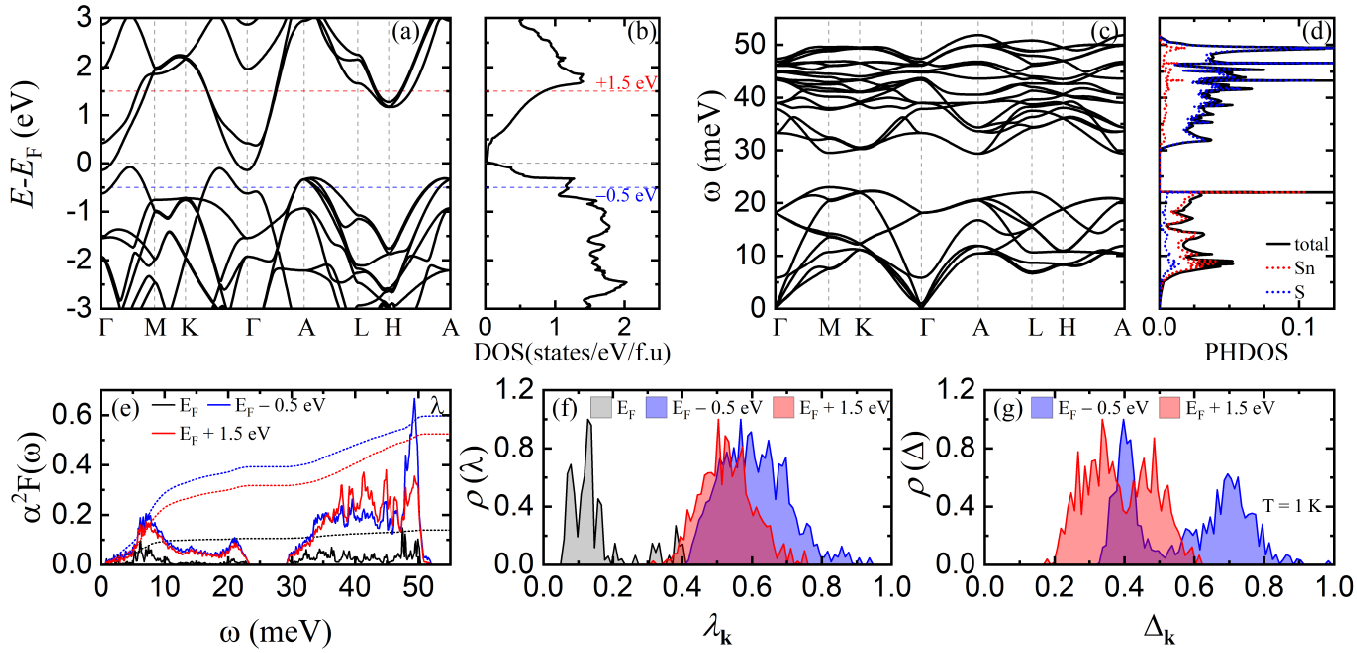

FIG. S22. Calculated (a) band structure, (b) DOS, (c) phonon dispersion, (d) PHDOS, (e) Eliashberg spectral function $\alpha^2F(\omega)$ and e-ph coupling strength $\lambda(\omega)$, (f) energy distribution of the e-ph coupling strength $\lambda_{\mathbf{k}}$, and (g) energy distribution of the superconducting gap $\Delta_{\mathbf{k}}$ at $T = 1$ K for the $H2$-1 structure in the $\sqrt{3} \times \sqrt{3} \times 1$ supercell of SnS_2 at 30 GPa. In (e)-(g), black lines show the quantities at the Fermi level, while red and blue lines correspond to the rigid shifts in the Fermi level indicated in (a) and (b). Note that the DOS and PHDOS are plotted per formula unit.

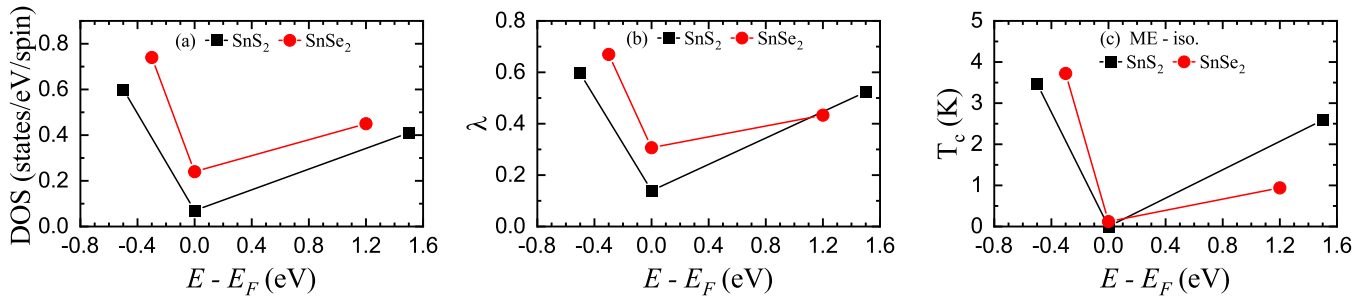

FIG. S23. Variations in (a) DOS at E_{F}, (b) λ, and (c) T_{c} as a function of a rigid shift of the Fermi level for the $H2$-1 structure in the $\sqrt{3} \times \sqrt{3} \times 1$ supercell of $SnSe_2$ (red lines and symbols) and SnS_2 (black lines and symbols) at 30 GPa. In (c), the T_{c} is obtained from the numerical solutions of the isotropic ME equations.

* rmargine@binghamton.edu

[1] J. Ying, H. Paudyal, C. Heil, X. J. Chen, V. V. Struzhkin, and E. R. Margine, "Unusual pressure-induced periodic lattice distortion in $SnSe_2$", Phys. Rev. Lett. **121**, 027003 (2018).
[2] Y. Zhou, B. Zhang, X. Chen, C. Gu, C. An, Y. Zhou, K. Cai, Y. Yuan, C. Chen, H. Wu, R. Zhang, C. Park, Y. Xiong, X. Zhang, K. Wang, and Z. Yang, "Pressure-induced metallization and robust superconductivity in pristine $1T$-$SnSe_2$", Adv. Electron. Mater. **4**, 1800155 (2018).
[3] Z. V. Borges, C. M. Poffo, J. C. de Lima, S. M. Souza, D. M. Trichôs, and R. S. de Biasi, "High-pressure angle-dispersive X-ray diffraction study of mechanically alloyed $SnSe_2$", J. Appl. Phys. **124**, 215901 (2018).
[4] K. Knorr, L. Ehm, M. Hytha, B. Winkler, and W. Depmeier, "The High pressure behaviour of SnS_2: X-Ray powder diffraction and quantum mechanical calculations up to 10 GPa", Phys. Stat. Sol. **223**, 435 (2001).
[5] R. M. Hazen, L. W. Finger, "The crystal structures and compressibilities of layer minerals at high pressure. I. SnS_2, berndtite", American Mineralogist **63**, 289 (1978).
[6] M. Ø. Filsø, E. Eikeland, J. Zhang, S. R. Madsen and B. B. Iversen, "Atomic and electronic structure transformations in SnS_2 at high pressures: a joint single crystal X-ray diffraction and DFT study", Dalton Trans. **45**, 3798 (2016).
[7] SPGLIB, https://spglib.github.io/spglib/.
[8] S. Hajinazar, A. Thorn, E. D. Sandoval, S. Kharabadze, and A. N. Kolmogorova, "MAISE: Construction of neural network interatomic models and evolutionary structure optimization", arXiv:2005.12131v2.